

Interfacial reaction of Co–Fe films with SiO₂ substrates

L.A. Bendersky^{a,*}, N.V. Kazantseva^{a,c}, U.R. Kattner^a, K. Wang^a, V.P. Oleshko^a,
D. Hunter^b, I. Takeuchi^b

^a Material Measurement Laboratory, National Institute of Standards and Technology, Gaithersburg, MD 20899, USA

^b Department of Material Science and Engineering, University of Maryland, College Park, MD 20742, USA

^c Institute of Metal Physics, Urals Branch of the Academy of Sciences, Ekaterinburg 620219, Russia

Received 29 January 2013; received in revised form 25 March 2013; accepted 27 March 2013

Available online 27 April 2013

Abstract

The interdiffusion reaction between Co_{1-x}Fe_x deposited films of various compositions ($x = 0.27, 0.32$ and 0.50) and an amorphous SiO₂ substrate during annealing in vacuum at 800 °C was identified by analytical transmission electron microscopy. The reaction results in the formation of Fe₂SiO₄ mixed silicate of olivine structure as an interfacial phase. The following microstructural changes occurring during this reaction are inferred: (a) recrystallization of as-deposited films during the 800 °C annealing results in large grains of the body centered cubic Co–Fe solid solution; (b) metals diffuse into the SiO₂ substrate and nucleate grains of the Fe₂SiO₄ silicate along the film/SiO₂ interface; (c) silicon and oxygen partially released during the reaction, in turn, diffuse into an unreacted metallic film and form precipitates of the (Co,Fe)₃O₄ spinel phase and solid solution of Si in Co–Fe. To our best knowledge, the formation of silicates with olivine-type structure (known as fayalite for Fe) as products of the metal/SiO₂ reaction has never been reported before. Thermodynamic evaluation of the reaction employing the semi-empirical CALPHAD (Calculation of Phase Diagrams) method supports the experimental findings, although the reaction requires an excess of oxygen.

Published by Elsevier Ltd. on behalf of Acta Materialia Inc.

Keywords: Co–Fe films; Interfacial reaction; Fe₂SiO₄; Silicate SiO₂; TEM

1. Introduction

Reaction of metal films with SiO₂ has been of great interest for semiconductor technology and related research since 1970; understanding the reaction between refractory metals and SiO₂ is a critical factor in maintaining stability of devices and controlling the formation of new structures [1,2]. Refractory metal silicides have found wide application in advanced integrated circuit metallization because of their low resistivity and high thermal stability. During circuit fabrication, pure refractory metals are usually brought in contact with various dielectrics such as SiO₂ [3]. This method presents both opportunities and challenges for the manufacture of microelectronic devices, not

only for traditional microelectronics devices but also for novel devices that may incorporate quantum dots.

The reactions between thin refractory metal films and SiO₂ substrates under thermal anneal in vacuum at temperatures between 320 °C and 900 °C have been studied by different experimental techniques, mostly Rutherford backscattering and X-ray diffraction (XRD) [4,3,5–7]. It was found that some metals, e.g., Ti and Zr, react with SiO₂ and form silicides, whereas others such as Fe, Co and Ni do not [6]. The reaction of a thin metal (M) film with a SiO₂ substrate may result in the formation of both metal silicides and metal oxides, i.e., $M_x + SiO_2 \rightarrow M_ySi + M_{x-y}O_2$. Heats of the reaction were calculated for different combinations of silicide and metal–oxide reaction products, and in all cases metal–SiO₂ reactions only take place when the calculated heat of reaction is negative [6,7]. This study shows that the occurrence of the reaction correlates well with the electronegativity of the metal,

* Corresponding author. Tel.: +1 301 975 6167.

E-mail address: leoben@nist.gov (L.A. Bendersky).

which offers a convenient empirical method of predicting whether a metal will react with SiO₂ or not. No other products of the M_x + SiO₂ reaction, e.g., formation of silicates, were considered in these publications.

In our recent study of Co–Fe films on an amorphous SiO₂ substrate were investigated for their magnetostriction property; with a combinatorial approach a wide range of Co_{1–x}Fe_x compositions has been studied [8]. In the study significant increase in the films' magnetostriction after annealing at 800 °C has been discovered. Synchrotron XRD and transmission electron microscopy (TEM) of cross-sectional samples had identified the formation of an interfacial phase between SiO₂ and Co–Fe films after the annealing. This was a surprising discovery since, according to previous reports [6,7], no reaction between either Co or Fe and SiO₂ was predicted. However, it should be noted that the predictions were for the formation of M_xSi_y silicides; also only single metals and not binary alloys were considered in Refs. [6,7].

In this publication we present detailed microstructural TEM studies of the reactions between different Co_{1–x}Fe_x films (0.27 < x < 0.50) and an amorphous SiO₂ substrate. The interfacial phase was identified as a Fe₂SiO₄ silicate; to our best knowledge formation of silicates as a product of metal/SiO₂ reaction has never been reported before. Thermodynamic evaluation of the reaction employing the CALPHAD (Calculation of Phase Diagrams) method was conducted; results of the calculations support the experimental finding in general.

2. Experimental procedure

Thin film Co_{1–x}Fe_x binary composition spreads (thickness 0.5 ± 0.01 μm) were deposited at room temperature using an ultrahigh-vacuum magnetron sputtering system onto an array of cantilevers which had been patterned from a thermally oxidized (10.5 μm SiO₂) Si wafer (see details in Ref. [8]). After deposition, the Fe and Co concentration on each cantilever in the spread was mapped by wavelength dispersive spectroscopy analysis with a JEOL electron probe (JXA-8900R).¹ The compositional variation across each cantilever was less than 0.015 mol fraction. Some of the as-grown spreads were annealed at 800 °C for 1 h in a UHV vacuum chamber with a base pressure lower than 1 × 10^{–9} Pa. After annealing, the spreads were cooled from high temperature in vacuum either by slow-cooling or by the quenched method. For the slow-cool method the cooling rate was estimated to be ~5 °C min^{–1}; for the quenched method the cooling to room temperature occurred in less than 2 s.

For the TEM study, cantilevers with average compositions of 0.27, 0.32 and 0.50 Fe mole fraction of both as-deposited and annealed wafers were used to prepare both cross-sectional and plan-view TEM samples. The cross-sectional samples were prepared by gluing two films facing each other, mechanically thinning (grinding and dimpling) and finally ion milling to electron transparency by using a low-angle (<4°) 3 kV Ar ion beam at liquid-nitrogen temperature. The plan-view samples were prepared by one-side (substrate) grinding and dimpling followed by ion milling. The film side was always protected and only in the last few minutes of final ion milling was exposed to an ion beam.

The TEM samples were examined in JEOL JEM 3010 and Philips CM30 microscopes. Scanning TEM imaging and chemical analyses in the nanoprobe mode with ~0.2 nm probe were performed in an FEI Titan 80-300 AEM at 300 kV equipped with a Fischione high-angle annular dark-field (HAADF) detector, an EDAX Si/Li X-ray energy dispersive spectrometry (XEDS) detector and a Gatan Enfina electron energy-loss spectrometer (EELS). To ensure optimal counting rates, the TEM specimens were tilted 15° towards the XEDS detector. XEDS spectra have been quantified using a Cliff–Lorimer thin film ratio method with calculated *k* factors for Fe and Co, and absorption (mass thickness) correction with accuracy within ±20%, as described elsewhere [9]. The SiO₂ substrate (assumed stoichiometric) was utilized as an internal standard to obtain a relative *k* factor for silicon/oxygen, *k*_{Si}^O = 1.20; the experimental *k* factor allowed to minimize overestimation of oxygen within the film if using the calculated *k* factor (*k*_{Si}^O = 2.008). The local specimen thickness was determined by EELS using a log-ratio technique [10] and the obtained values were used then for calculations of absorption correction factors.

3. Results

Fig. 1 shows bright-field TEM images taken from cross-sectional samples of Co–0.32 Fe mole fraction and Co–0.50 Fe mole fraction films. Both images clearly show the presence of a continuous layer of ~70–100 nm thick (labeled as IRP for “interfacial reaction phase” in the figure) that separates a metal film from an amorphous SiO₂ substrate. The film consists of large grains of a body centered cubic (bcc) phase; the grain size is typically larger than the film thickness. The IRP layer is continuous and consists of block-like grains; the grains have a sharp, slightly undulating interface with the film and a wavy, ill-defined interface with SiO₂. The interface with SiO₂ has undulations of the order of 10 nm, which is less than the thickness of a typical TEM sample. Ridges and valleys of the interface's surface overlap in projection along the direction of an electron beam, thus the projected interface appears diffuse.

Selected area electron diffraction (SAED) patterns from a number of the IRP grains oriented to a low-index zone axis were recorded. Fig. 2a shows such an oriented grain (dark contrast due to multiple beam diffraction) in the

¹ Certain commercial equipment, instruments or materials are identified in this paper. Such identification does not imply recommendation or endorsement by the National Institute of Standards and Technology, nor does it imply that the products identified are necessarily the best available for the purpose.

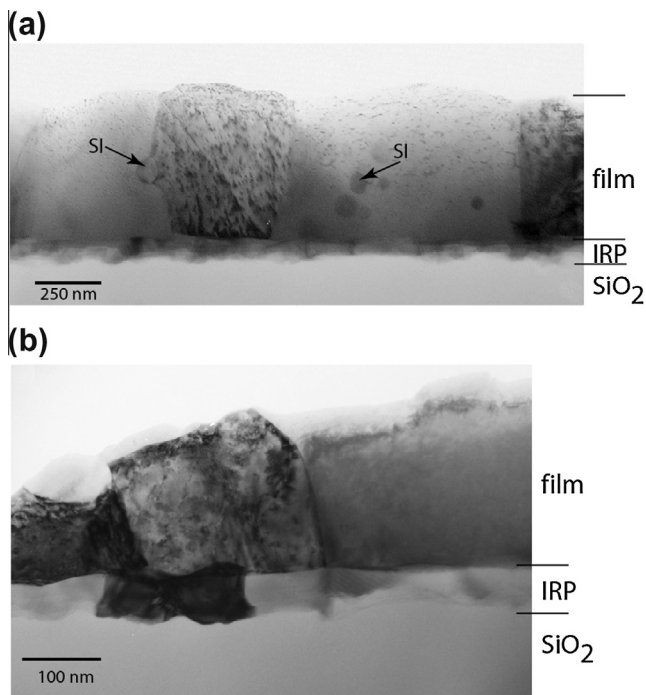


Fig. 1. Bright field TEM images from cross-sectional samples of films deposited with composition $\text{Co}_{1-x}\text{Fe}_x$ on SiO_2 substrates following high-temperature annealing at 800°C : (a) $x = 0.32$; (b) $x = 0.50$. The films exhibit spherical inclusions (SI) within the metal films and an interfacial reaction phase (IRP) at the film–substrate interface.

Co – 0.50 Fe mole fraction film from which the SAED pattern, Fig. 2b, was recorded. Another SAED pattern from the IRP of the Co – 0.32 Fe mole fraction film is shown in Fig. 2c. The patterns are indexed as belonging to $[110]$ (Fig. 2b) and $[211]$ (Fig. 2c) zone axes of an orthorhombic silicate with olivine structure (lattice parameters fit the Fe_2SiO_4 member of olivines known as fayalite). All other SAED patterns from IRP in different TEM samples of all film compositions were also indexed as having a structure of Fe_2SiO_4 ; no silicide phases were detected.

Fayalite is the iron-end member of the olivine group with formula A_2BX_4 , where X represents the four-coordinated anions, which usually are oxygen [11]. It belongs to the space group $Pbnm$, has stoichiometry Fe_2SiO_4 and lattice parameters $a = 0.482$ nm, $b = 1.048$ nm and $c = 0.609$ nm. The structure consists of isolated SiO_4 tetrahedra that bind to each other ionically with Fe cations occupying octahedral sites, Fig. 3.

After annealing at 800°C , a fine-grain structure of as-deposited films has significantly coarsened to large grains [8]. Diffraction from these grains yielded strong reflections of a bcc structure; typically weak diffuse scattering was also seen. Apparently, the diffuse scattering results from structural inhomogeneities distributed throughout the grains; the inhomogeneities are visible both by diffraction and absorption contrast for the grains oriented close to or away from Bragg conditions, respectively, see Fig. 1. The nature of the fine inhomogeneities in the Co –Fe bcc grains and its

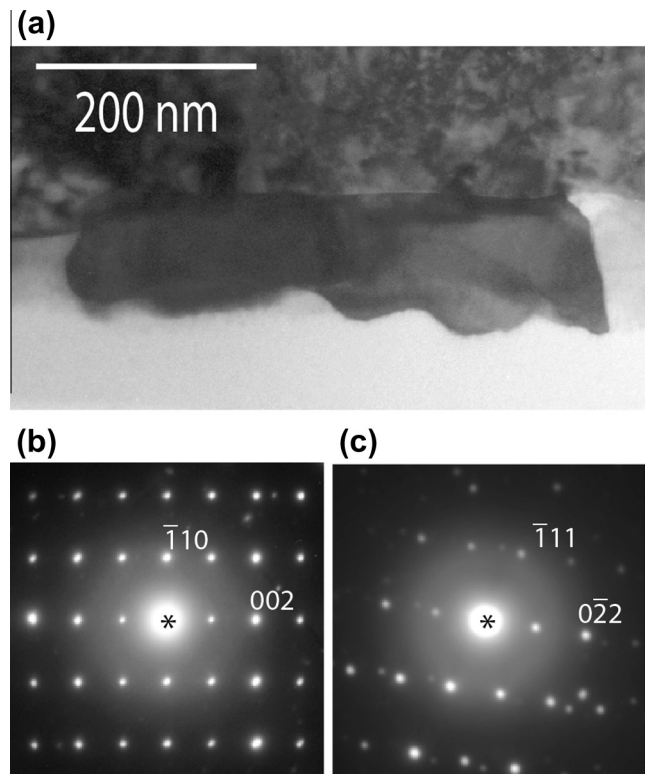


Fig. 2. (a) Bright field image of an oriented grain from a reaction zone in a cross-sectional sample of a film of composition $\text{Co}_{1-x}\text{Fe}_x$ with $x = 0.5$. (b, c) SAED patterns from IRP grains indexed as $[110]$ and $[211]$ of an orthorhombic Fe_2SiO_4 olivine structure. Kinematically forbidden reflections (b) 001 and (c) $0\bar{1}1$ appear in the patterns through double diffraction.

relation to the Co –Fe phase diagram will be discussed in a separate publication.

In addition, spherical inclusions labeled as SI in Fig. 1a can be seen inside the bcc grains. The distribution and morphology of these particles are best recognized in plan-view TEM samples (Fig. 4a): the inclusions size ranges from 20 nm to 60 nm and the inclusions can be found both in the grains' interior and boundaries. From SAED patterns the inclusions are identified as a face centered cubic (fcc) phase with $a \approx 0.84$ nm; examples of these SAED patterns are presented in Fig. 4b and c. The lattice parameter, Bravais lattice and observed extinctions of reflections fit well with the spinel structure of either CoFe_2O_4 or Fe_3O_4 . Similar spherical spinel particles were observed in $(\text{Fe}_{0.65}\text{Co}_{0.35})\text{O}$ thin films prepared by RF reactive magnetron sputtering with $\text{Ar} + \text{O}_2$ gases and annealed at 480°C [12]; in the paper the improvement in soft magnetic properties of the annealed films was attributed to the formation of CoFe_2O_4 nanoparticles.

To verify the conclusions derived from electron diffraction analysis on the nature of the interfacial reaction phases, analytical STEM measurements were conducted. An HAADF image from the cross-sectional Co – 0.32 Fe mole fraction sample shows a film/substrate interface in Fig. 5a; a series of XEDS spectra from spots 1 to 4 in

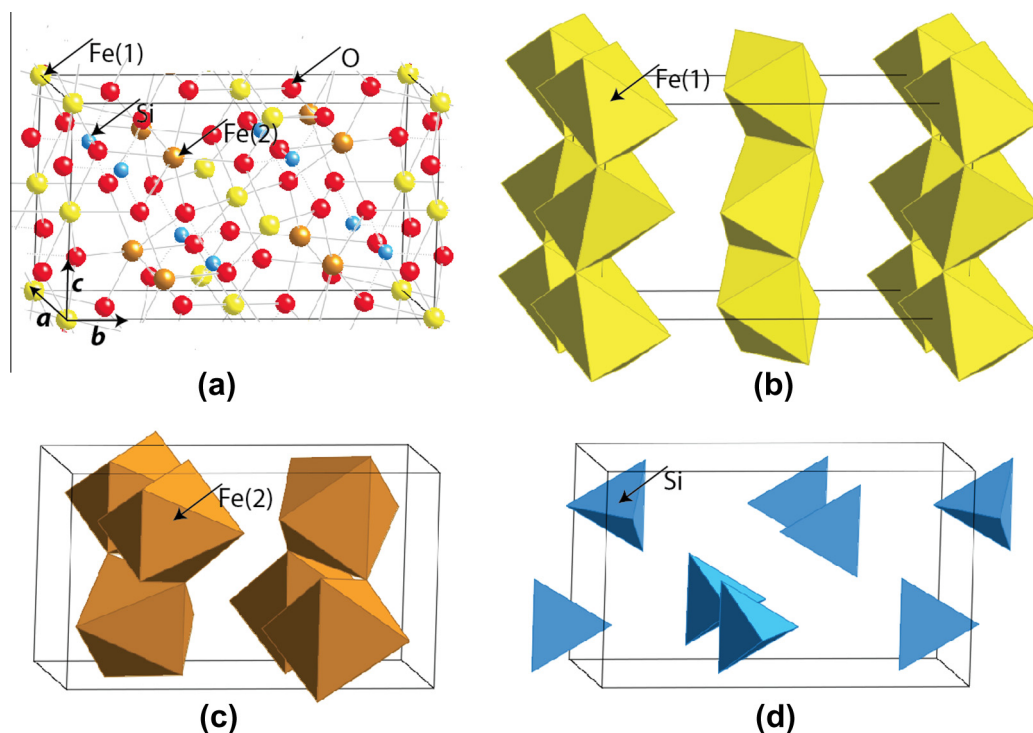


Fig. 3. Schematic drawings of the Fe_2SiO_4 olivine structure: (a) atomic positions within the unit cell; (b) the polyhedral framework of edge-sharing $\text{Fe}(1)\text{O}_6$ octahedra; (c) the polyhedral framework of corner-sharing $\text{Fe}(2)\text{O}_6$ octahedra; (d) the framework of isolated SiO_4 tetrahedra.

the image are also shown. The HAADF STEM image is mostly sensitive to average mass density (Z contrast) and demonstrates the lowest density for the SiO_2 substrate, higher density for both the IRP layer and the spherical inclusions and highest for the metallic film, which is consistent with the chemistry of phases established by diffraction analysis.

Table 1 compiles the results of quantitative compositional XEDS for the four selected spots using a Cliff–Lorimer thin film ratio technique. The composition of the substrate (point 4, also employed as an internal standard) was estimated as $\text{Si}_{0.36}\text{O}_{0.64}$ by XEDS and $\text{Si}_{0.37}\text{O}_{0.63}$ by EELS, respectively, which is close to the expected stoichiometric SiO_2 . The use of SiO_2 as an internal standard for the k_{Si}^{O} factor minimized overestimation of oxygen within the metallic film as compared to the calculated k factor and gave reasonably good agreement for the values of Co/Fe ratios obtained independently by XEDS and EELS from the same spots for the oxide inclusion (spot 1), the Co–Fe matrix (spot 2) and the IRP zone (spot 3). The composition of the IRP (point 3) was close within 8% to $(\text{M})_2\text{SiO}_4$, with combined $\text{M} = (\text{Fe} + \text{Co}) = 0.366\%$, $\text{Si} = 0.144$ and $\text{O} = 0.49$ mol fraction, as compared to 0.286, 0.143% and 0.571 of the stoichiometry, respectively. The Co/Fe ratio is significantly less than for the nominal film’s composition 2.1, which suggests that the IRP is Fe_2SiO_4 fayalite with minor solubility of Co– $(\text{Fe}(\text{Co}))_2\text{SiO}_4$. The composition of the Co–0.32 Fe mole fraction film at point 2 (~ 50 nm away from the reaction layer) shows Co/Fe = 1.7, which is less than the expected value of 2.1;

considering dilution of the film in Fe resulting from the formation of Fe-rich IRP, the opposite would be expected. The relatively high level of oxygen in the point 2, 0.10 mol fraction is attributed to the surface oxidation of the TEM sample and to uncertainties in the deconvolution procedure required for determination of integral net counts of the oxygen X-ray signals as well. In this case, the low intensity O $\text{K}\alpha_1$ peak at 0.523 keV appeared as a shoulder strongly overlapped with the Fe L series (the Fe $\text{L}\alpha_1$ peak at 0.704 keV) and the Co L series (the Co $\text{L}\alpha_1$ peak at 0.775 keV), respectively. The composition at point 1 has 0.28 mol fraction O, which is less than for the stoichiometry of spinel $(\text{Fe},\text{Co})_3\text{O}_4$, which suggests significant overlap of the matrix and the inclusion phases along the electron beam direction. Overall, because of such compositional non-uniformity and the absence of a full standard set for the XEDS measurements, quantification of the XEDS results should be considered only as a first approximation.

Conclusions from the point measurements were corroborated by the Z -contrast HAADF STEM imaging coupled with drift corrected X-ray spectral line profiling across the features of interest, Fig. 6. The line profile across a spherical oxide inclusion in the Co–Fe matrix acquired in the nanoprobe mode is shown in Fig. 6a for the Co–0.32 Fe mole fraction film; the profile shows the decrease in Co and increase in Fe in comparison to the surrounding matrix. From these measurements the presence of Co in the M_3O_4 spinel is uncertain, hence the proposed $(\text{Co},\text{Fe})_3\text{O}_4$ stoichiometry. The HAADF image and XEDS line profile across the interfacial phase, IRP, in the Co–0.50 Fe

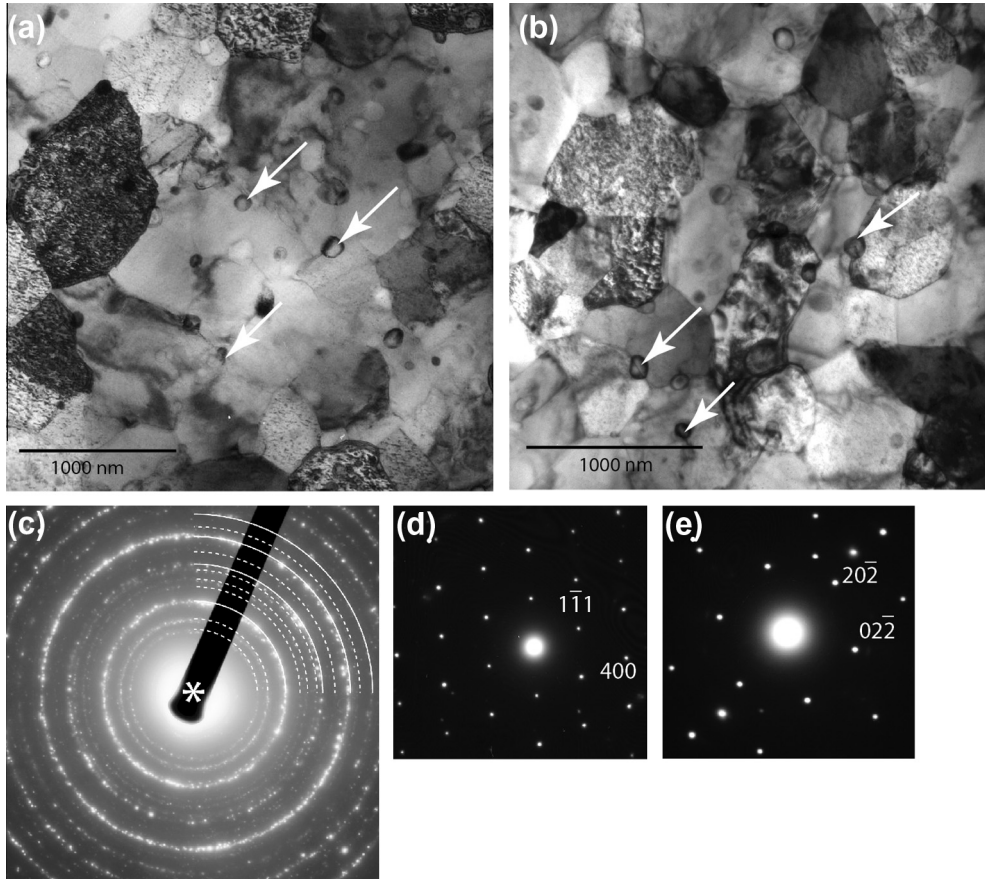


Fig. 4. Bright field images from plan-view samples of composition $\text{Co}_{1-x}\text{Fe}_x$ with $x = 0.32$ (a) and $x = 0.5$ (b); white arrows point on the spherical inclusions; (c) SAED pattern taken with a very large SAD aperture exhibits rings of reflections. The rings are indexed as bcc Fe–Co (continuous lines) and $(\text{Co,Fe})_3\text{O}_4$ (dashed lines); SAED patterns from individual inclusions are indexed as (d) $[0\ 1\ 1]$ and (e) $[1\ 1\ 1]$ of a cubic spinel structure $(\text{Co,Fe})_3\text{O}_4$.

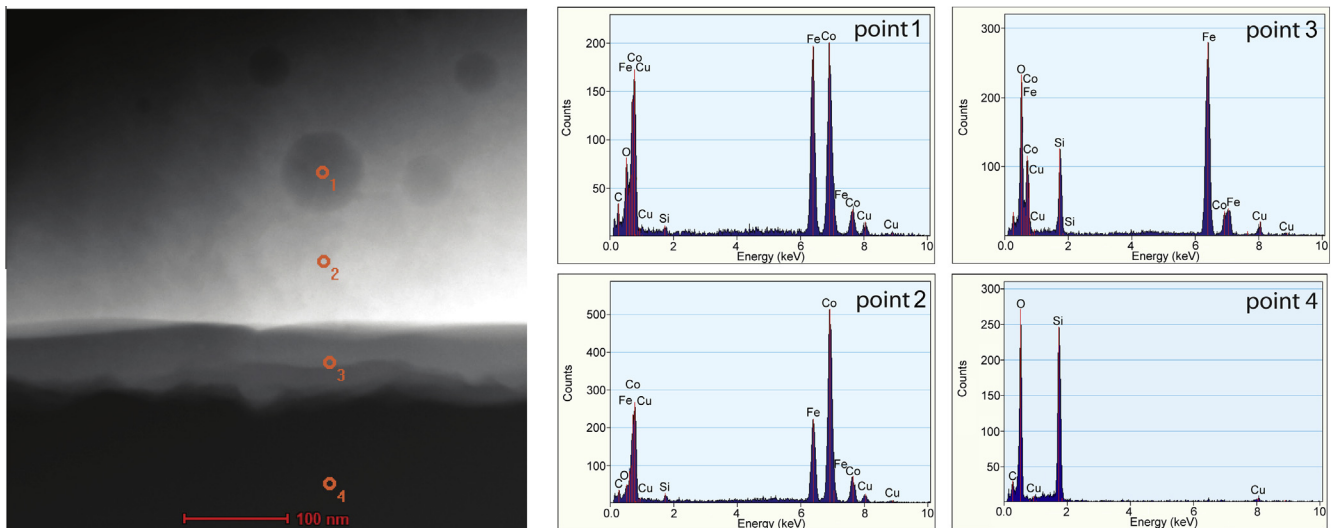


Fig. 5. STEM-HAADF image and XEDS point spectra from the cross-sectional TEM sample of initial composition $\text{Co}_{1-x}\text{Fe}_x$ with $x = 0.32$.

mole fraction film is shown in Fig. 6b. The HAADF intensity clearly follows the compositional changes of the major constituents in the XEDS line profile. The profile shows an abrupt decrease in Co (almost to zero) and Fe at the film/

IRP interface, which supports the previous conclusion that the interfacial reaction phase is Fe-dominated fayalite. Based on the profiles of Fe, Co and Si the boundaries of the IRP can be clearly determined. In addition, the pres-

Table 1

Spot XEDS and EELS analyses of a cross section of the Co–32 at.% Fe alloy. The EDXS results are compared with stoichiometric compositions of the phases. The error in concentration is represented by the standard deviation 2σ corresponding to the confidence limit of 95%.

Point	Description	Composition, mole fraction, from EDXS				Ratio of elements	
		Fe	Co	Si	O	XEDS	EELS
1	Spinel inclusion embedded in a Co–Fe matrix	0.36 ± 0.02	0.35 ± 0.08	0.01 ± 0.01	0.28 ± 0.09	0.96 ± 0.06 (Co/Fe)	1.0 ± 0.1 (Co/Fe)
	CoFe ₂ O ₄	0.429	–	–	0.57	–	–
2	Co–Fe matrix near the reactive zone	0.33 ± 0.02	0.56 ± 0.02	0.01 ± 0.01	0.11 ± 0.01	1.7 ± 0.3 (Co/Fe)	1.7 ± 0.1 (Co/Fe)
	Nominal composition of the film	0.32	0.68	–	–	–	–
3	Layer of IRP	0.34 ± 0.07	0.03 ± 0.04	0.14 ± 0.05	0.49 ± 0.05	0.08 ± 0.01 (Co/Fe)	0.10 ± 0.02 (Co/Fe)
	Fe ₂ SiO ₄	0.286	–	0.143	0.571	–	–
4	Amorphous SiO ₂ substrate	>0.001	>0.001	0.36 ± 0.01	0.64 ± 0.01	0.55 ± 0.07 (Si/O)	0.57 ± 0.08 (Si/O)
	SiO ₂	–	–	0.33	0.66	–	–

ence of Si throughout the film (from 0.007 to 0.02 mol fraction) was measured for all films studied.

4. Discussion

In this work, a large number of Co_{1-x}Fe_x deposited films of various compositions ($0.27 < x < 0.50$) deposited on amorphous SiO₂ substrates and annealed at 800 °C for 1 h were examined by TEM/STEM. Based on these results, we offer the following picture of structural changes that occurred during 800 °C annealing:

1. The fine-grain structure of as-deposited films quickly recrystallizes and forms large grains of the bcc Co–Fe solid solution.
2. Fe (and to some extent Co) reacts with SiO₂ and nucleates grains of the (Fe(Co))₂SiO₄ silicate along the film/SiO₂ interface. Considering the amorphous nature of SiO₂ and the lack of structural relationship between bcc Co–Fe and silicate phases, the orientation of the nucleated phase is random. The (Fe(Co))₂SiO₄ grains coalesce and form a continuous layer separating the SiO₂ substrate and metallic film.
3. The Fe(Co) + SiO₂ reaction releases unbounded Si and O that diffuse into an unreacted metallic film. Since solubility of oxygen in Fe or Co is very low [13,14], precipitation of the (Co,Fe)₃O₄ (spinel) occurs throughout the film; coarsening forms round particles of the oxide. Si has solubility in the bcc Fe,Co, as well as high diffusivity, and a low concentration (0.01–0.02 mol fraction) of Si is uniformly distributed in the film [15].
4. Since both reaction products Fe(Co)₂SiO₄ and (Co,Fe)₃O₄ are enriched in Fe, the composition of the bcc Co–Fe films after the interfacial reaction is shifted to higher Co concentration. Higher Co concentration may result in the precipitation of an fcc phase during cooling from 800 °C [16].

Formation of a silicate phase with olivine-type structure (known as fayalite for Fe) resulting from a diffusion reac-

tion between metallic film and SiO₂ was never reported before, to our knowledge. A general crystallo-chemical formula for olivine-type compounds is (M1)(M2)TO₄, where M1 and M2 represent octahedrally coordinated cations, see Fig. 3a, and T is the cation tetrahedrally coordinated by oxygen, see Fig. 3b. For T = Si (silicate) there are a number of natural and synthetic olivine compounds with M1 and M2, including Mg, Li, Ca and different transition metals [17]. The magnetic properties of M₂SiO₄ (M = Co, Fe, Ni and Mn) have been studied by different groups, all of which are antiferromagnetic (AF) at sufficiently low temperatures [18,19].

According to the literature, no reaction between pure Fe or Co films and SiO₂ (fused quartz) was experimentally measured after annealing under vacuum at 800 °C [6]; these results contradict our finding. Pretorius et al. [6,7] have supported their experimental results by thermodynamic evaluation of the chemical reaction SiO₂ + M_x = M_ySi + M_{x-y}O₂: when heat of reaction ΔH is positive, the reaction would not occur. For Co and Fe ΔH was calculated as +38.1 kJ mol⁻¹ to 79.5 kJ mol⁻¹ (+9.1 to +19 kcal g⁻¹ atom⁻¹) and +27.6 kJ mol⁻¹ to 28.8 kJ mol⁻¹ (+6.6 to +6.8 kcal g⁻¹ atom⁻¹), respectively (the range of values is for different combinations of different silicides and oxides). However, these calculations are not directly applicable to our results since the products of the SiO₂ + M_x reaction are different: e.g. 2Fe + 2SiO₂ = Fe₂SiO₄ + Si. It should be noted that no TEM study was performed in Refs. [6,7] and it is possible that the small volume of a reaction product was missed by XRD and RBS; note that in our previous study of the same samples the reaction phases were also not detected by XRD [8].

The limitations of the thermodynamic evaluation by Pretorius et al. [6,7] are that only stoichiometric reactions were taken into account, no temperature dependence was considered and the overall Gibbs energy of the system was not minimized. These limitations can be overcome by performing thermodynamic calculations employing the CALPHAD method [20]. The CALPHAD method is a semi-empirical method where the Gibbs energy functions

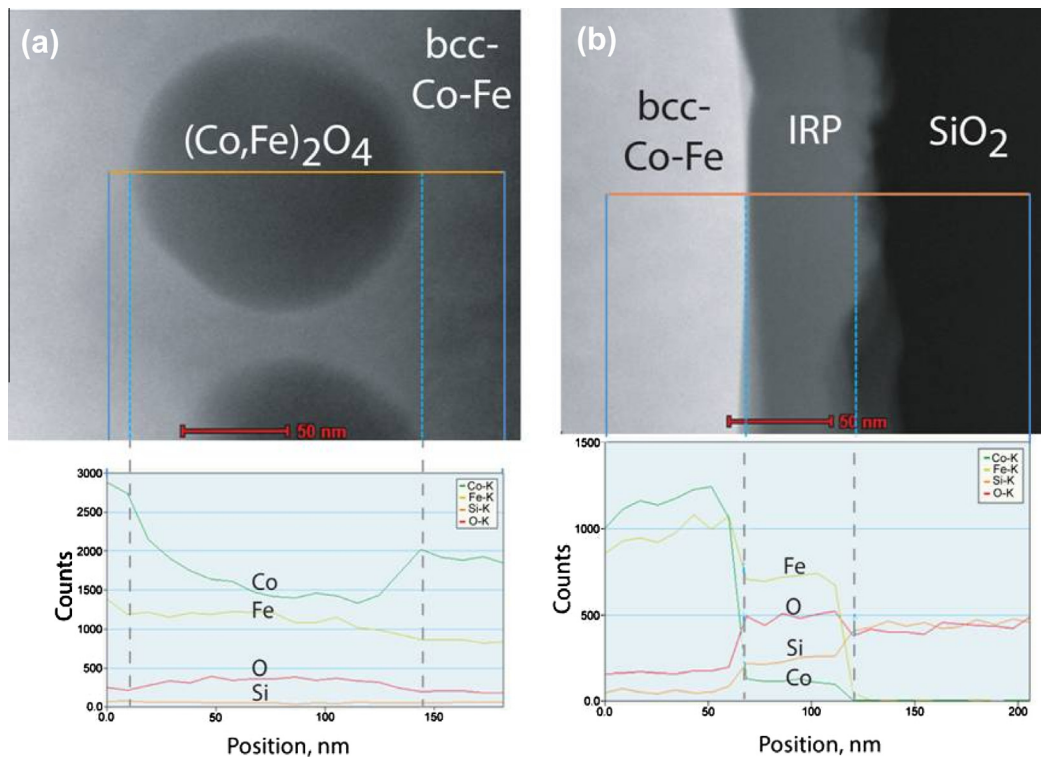


Fig. 6. STEM-HAADF images and drift-corrected XEDS compositional line profiles: (a) oxide spherical inclusion (SI) within a Co–Fe film, $x = 0.32$; (b) reaction layer (IRP) separating a Co–Fe film and a SiO_2 substrate, $x = 0.50$.

of each phase is described as functions of temperature, composition and, if needed, pressure, and the equilibrium is determined from a global minimization for given conditions. The CALPHAD calculations and their results are described in detail in the [Appendix A](#).

The calculations show that olivine forms from the reaction of the Fe,Co alloy and SiO_2 ; the reaction also enriched the alloy in Co and dissolves Si in the alloy. The Si solubility of the alloy in equilibrium with olivine and SiO_2 is extremely small and, therefore, the amount of olivine formed is also extremely small. However, it is possible that, because of film size effects, the Gibbs energy functions are altered and result in enhanced solubilities compared to the bulk phases [21]. Olivine formation will increase only in the presence of excess oxygen; only after the SiO_2 has been consumed will the silicate form. Since the supply of SiO_2 is large in comparison with the amount of the alloy, the calculations predict that the oxide formation cannot originate from SiO_2 consumption. Thus, excess oxygen within the alloy film or in the ambient atmosphere has to be a potential cause for the precipitation of the oxide particles. However, the source of this excess oxygen is unclear because of the high vacuum that has been used during sample preparation and annealing. The need for excess oxygen to allow the formation of the olivine and oxide phases is also evident from the isothermal sections of Fe–Si–O and Co–Si–O phase diagrams, as shown in the [Appendix A](#).

The results of the calculations also show that a Fe-rich olivine is in equilibrium with a Co-enriched alloy. The fact

that $(\text{Co,Fe})_3\text{O}_4$ (magnetite) is experimentally observed in the alloy matrix but the calculation shows high-temperature ($>555^\circ\text{C}$) $(\text{Co,Fe})\text{O}$ (wustite) as the stable oxide phase at 800°C could be attributed to two scenarios: (1) the high-temperature $(\text{Co,Fe})\text{O}$ phase decomposed during cooling into bcc and $(\text{Co,Fe})_3\text{O}_4$ or (2) $(\text{Co,Fe})\text{O}$ did not form as a result of nucleation difficulties or increased surface energies compared to $(\text{Co,Fe})_3\text{O}_4$. The observed microstructures, e.g. those shown in [Fig. 4](#), do not give an indication which scenario occurred since it is possible that the bcc phase formed during the decomposition of $(\text{Co,Fe})\text{O}$ was absorbed by the alloy matrix.

The results clearly support the possibility that olivine can form from a diffusion reaction between metallic film and SiO_2 . However, it should be noted that the calculations also show that significant phase amounts are only produced by this reaction when oxygen is present in excess to the O/Si ratio of 2/1 of SiO_2 . The presence of external oxygen excess is not supported by experimental conditions: the annealing experiments were performed in high vacuum and the same reaction (although without spinel phase) was observed in the control annealing experiments performed in high-vacuum RTA furnace. The possibility of the excess of oxygen in SiO_2 is also difficult to explain since usually non-stoichiometric silica is deficient in oxygen [22]. However, the excess of oxygen could be supplied by the formation of sub-stoichiometric $\text{SiO}_{2-\delta}$, e.g., in the reaction $2\text{Fe} + 4\text{SiO}_2 = \text{Fe}_2\text{SiO}_4 + \text{Si} + 2\text{SiO}_{2-\delta} + 0.2\delta\text{O}$. Recent work on FeCo– SiO_2 granular films annealed at 450–

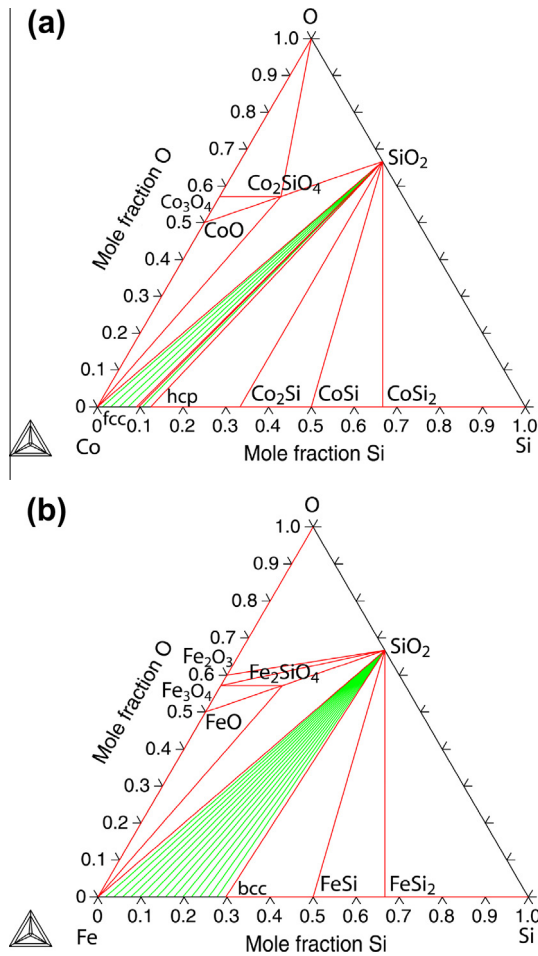


Fig. A1. Calculated isothermal sections at 800 °C. (a) Co–Si–O and (b) Fe–Si–O.

700 °C also demonstrated the formation of Co_3O_4 and CoFe_2O_4 phases [23]. Thus, even CALPHAD calculations supported the possibility of the observed reaction; there is no full correspondence with the experiment. It should be also noted that it is possible to suppress this diffusion reaction by the addition of a small amount of excess silicon to the alloy.

5. Conclusions

In this work, we demonstrate that the reaction between $\text{Co}_{1-x}\text{Fe}_x$ deposited films of various compositions ($x = 0.27, 0.32$ and 0.50) and an amorphous SiO_2 substrate during annealing in vacuum at 800 °C can occur. The reac-

tion results in the formation of Fe-rich $(\text{Fe}(\text{Co}))_2\text{SiO}_4$ olivine silicate as an interfacial phase. The microstructural changes occurring during this reaction in the metallic film and at the film/ SiO_2 interface have been characterized by analytical TEM. Our results show that a series of microstructural transformations occur during the reaction as follows:

- as-deposited films quickly recrystallize during annealing forming large bcc grains of the Co–Fe solid solution;
- metals (preferentially Fe) diffuse into the SiO_2 substrate and nucleate grains of the $(\text{Fe}(\text{Co}))_2\text{SiO}_4$ silicate along the film/ SiO_2 interface;
- silicon and oxygen released during the reaction, in turn, diffuse into an unreacted metallic film, resulting in precipitation of the $(\text{Co},\text{Fe})_3\text{O}_4$ spinel round particles, solid solution of Si in Co–Fe and, possibly, the formation of sub-stoichiometric SiO_2 .

To our best knowledge, the formation of silicates with olivine-type structure as products of the Fe,Co/ SiO_2 reaction has never been reported before. Thermodynamic evaluation of the reaction employing the semi-empirical CALPHAD method in general supports the experimental findings. However, not all details of the experimental work found explanation in the CALPHAD calculations, in particular the need for the excess of oxygen and formation of magnetite oxide (spinel) instead of wustite.

Acknowledgements

VPO gratefully acknowledges the support from the NIST (Contracts SB134110SE0579, SB134111SE0814 and Grant MML12-1053-N00). Robert Parke from NIST is acknowledged for assistance with TEM sample preparation.

Appendix A.

The present calculations were carried out with the Thermo-Calc software package [24]. The most complete description of the Co–Fe– Fe_2O_3 – SiO_2 system has been published by Jung et al. [25]. However, it was not possible to reproduce the calculations with the values found in the referenced literature since some of the referenced thermodynamic functions are part of a proprietary database that

Table A1
Gibbs energy parameters derived by the present work (Thermo-Calc notation [34] used, y_i^j is the concentration of species i on sublattice s).

Phase	Model	Parameter	Value (J mol^{-1})
(Co,Fe)Si	(Co,Fe)Si	$y_{\text{Co}}^1 y_{\text{Fe}}^1 L_{\text{Co,Fe:Si}}^0$	+3000
(Co,Fe)O	(Co,Fe)O	$y_{\text{Co}}^1 y_{\text{Fe}}^1 L_{\text{Co,Fe:O}}^0$	+10,000
(Co,Fe) $_3\text{O}_4$	(Co,Fe)(Co,Fe) $_2\text{O}_4$	$y_{\text{Fe}}^1 y_{\text{Co}}^2 G_{\text{Fe:Co:O}}$	$G_{\text{CoFe}_2\text{O}_4} + 100,000 - 30 * T$
		$y_{\text{Co}}^1 y_{\text{Fe}}^1 G_{\text{Co,Fe:*:O}}$	+10,000
		$y_{\text{Co}}^2 y_{\text{Fe}}^2 G_{*: \text{Co,Fe:O}}$	+10000

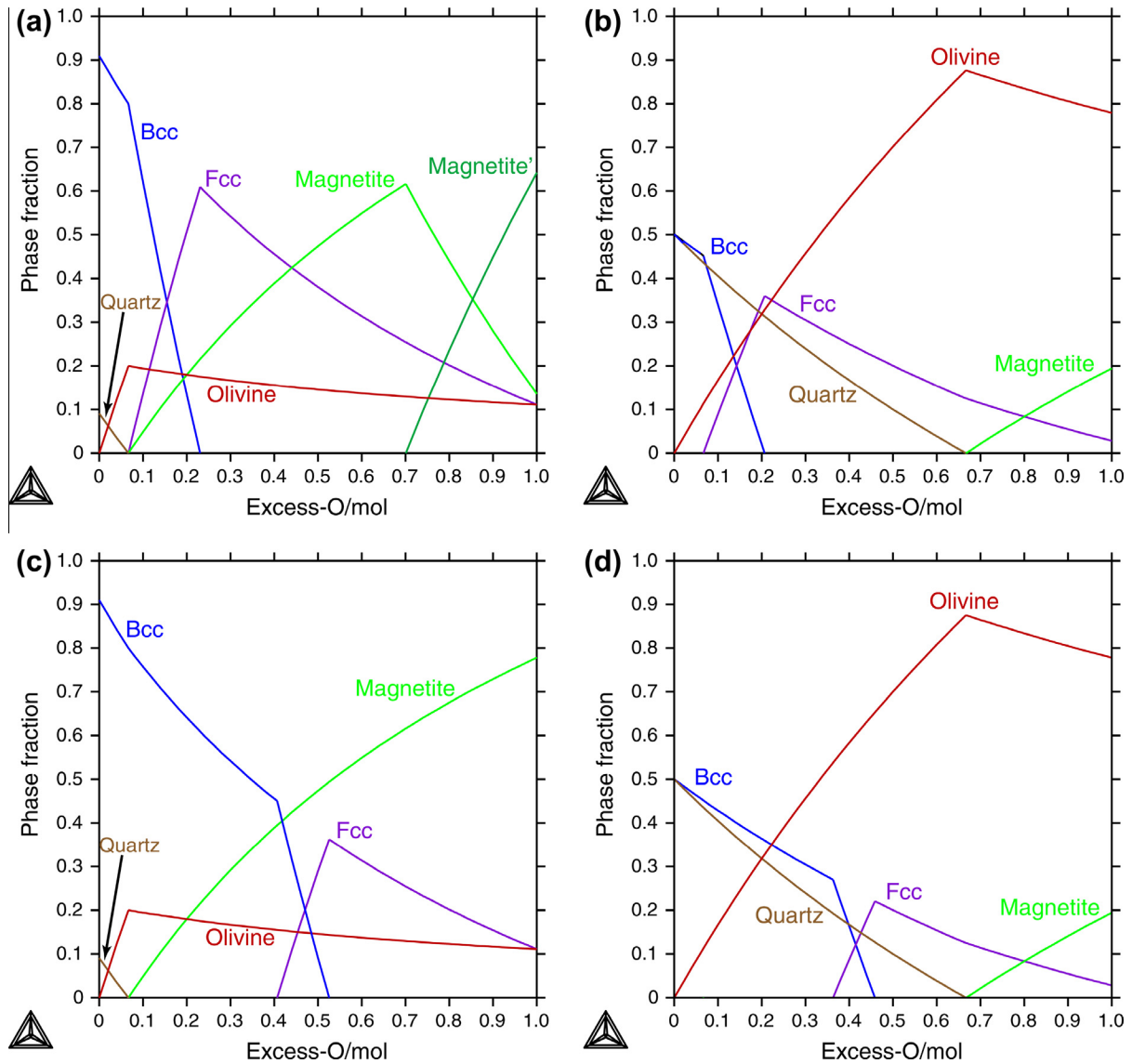


Fig. A2. Calculated phase fractions as function of excess oxygen. (a) 1 mol Co-32Fe + 0.1 mol SiO₂, (b) 1 mol Co-32Fe + 1 mol SiO₂, (c and a) 1 mol Co-50Fe + 0.1 mol SiO₂, (d and a) 1 mol Co-50Fe + 1 mol SiO₂.

was not available to the authors. Therefore, descriptions from the SGTE (Scientific Group Thermodata Europe) pure substances [26] and binary systems databases [27] were used for the construction of a thermodynamic database for the solid phases in the Co-Fe-Si-O system. The descriptions of the binary Co-Fe, Co-Si and Fe-Si systems were obtained from the binary systems database. The binary descriptions of the disordered solution phases, liquid, fcc, bcc and hexagonal close packed (hcp), were combined to represent the ternary interactions to extrapolate the thermodynamic properties of these phases to the ternary system. The description of the CoSi and FeSi binary phases were combined into the description of a semi-stoichiometric phase (Co,Fe)Si to reflect the continuous solubility of this phase in the ternary Co-Fe-Si system. The Gibbs energy function of the stoichiometric oxide phases, CoO, Co₃O₄, FeO, Fe₃O₄, Fe₂O₃, SiO₂, CoFe₂O₄, Co₂SiO₄ and

Fe₂SiO₄ were obtained from the pure substances database. To represent amorphous SiO₂ the description of liquid SiO₂ was used. The Gibbs energy values obtained from this description are in perfect agreement with the data given by Gurvich et al. [28] for vitreous SiO₂. The descriptions of CoO and FeO were combined into the description of a semi-stoichiometric phase (Co,Fe)O, Co₃O₄, Fe₃O₄, CoFe₂O₄ were combined into (Co,Fe)(Co,Fe)₂O₄, and Co₂SiO₄ and Fe₂SiO₄ were combined into (Co,Fe)₂SiO₄ to reflect their respective ternary and quaternary homogeneity ranges. Regular solution parameters for the interaction between Co and Fe were introduced to reproduce the ternary phase diagrams between 700 °C and 900 °C (Co-Fe-O [29], Co-Fe-Si [30], Fe-Si-O [31]). The calculated isothermal sections at 800 °C of the Co-Si-O and Fe-Si-O systems are shown in Fig. A1. The parameters for the end-member phase FeCo₂O₄ were estimated using the

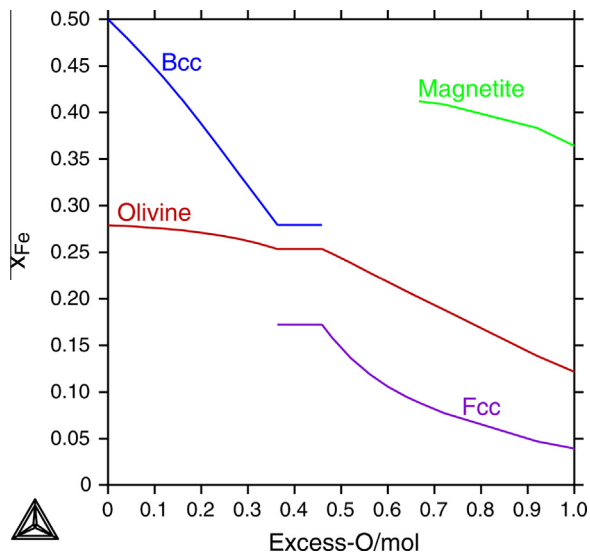


Fig. A3. Calculated Fe concentration in the phases for 1 mol Co–50Fe with 1 mol SiO₂ as function of excess oxygen in the system.

parameters of the CoFe₂O₄ phase and the exchange energies from Sundman [32] and Chen et al. [33]. The parameters derived in the present work are listed in Table A1. Even though interaction parameters were introduced in the present descriptions of the solution phases of the Co–Fe–Si–O system, the results of the calculations are basically the result of an extrapolation of the thermodynamic properties of the binary systems and the end-member phases and further refinement will be needed to accurately describe the system. However, the present description allows the calculation of the general features of the phase equilibria in this system.

This description was used to perform a series of calculations to examine the condition under which the olivine and oxide phases are formed. The calculation for compositions corresponding to a mixture of pure metal (Co,Fe) and pure SiO₂ showed that a small amount of Si was dissolved in the metal ($<10^{-10}$ mol) and a small amount of olivine (phase fraction $<10^{-10}$) and no oxide was formed. After adding excess oxygen to the overall composition olivine was formed; the effect of oxygen is also obvious from the phase diagrams in Fig. A1 – the two-phase equilibrium (Fe,Co)–SiO₂ is changing to the three-phase equilibrium (Fe,Co)–SiO₂–Fe₂SiO₄. The amount of olivine increased with increasing oxygen concentration and consuming SiO₂ only after SiO₂ was consumed the oxide phase began to form. The equilibrium oxide phase that forms at 800 °C is the (Co,Fe)O monoxide. However, since magnetite and not the monoxide was observed in the experiments, calculations in which the monoxide phase was suspended were also carried out. These calculations showed that magnetite also formed only after all SiO₂ was consumed by the formation of olivine. The general reaction mechanisms did not change whether the monoxide was allowed to form or not. The only difference was in the phase fractions of the oxide phases as a result

of the different stoichiometries. The phase fractions as function of excess oxygen are shown in Fig. A2 for the reacting 1 mol Co–0.32 Fe and 1 mol Co–0.50 Fe with 0.1 mol and 1 mol SiO₂, respectively. The Fe concentrations in the different phases for Co–0.50 Fe with 1 mol SiO₂ as a function of excess oxygen in the system are shown in Fig. A3. The calculation shows that both the olivine and the oxide are enriched in Fe (the maximum possible Fe concentration in olivine is 0.286 and in magnetite it is 0.429) and as more olivine and oxide are formed the metal becomes increasingly depleted in Fe. The calculations also show that with decreasing Fe concentration in the metal phase the formation of Co-rich fcc phase occurs.

References

- [1] Poate JW, Tu KN, Mayer JW, editors. Thin films – interdiffusion and reactions. New York: Wiley; 1978.
- [2] Murarka SP. Vac Sci Technol 1980;17:775.
- [3] Wang SQ, Mayer JW. J Appl Phys 1988;64:4711.
- [4] Krautle H, Nicolet M-A, Mayer JW. J. Appl. Phys. 1974;45:3304.
- [5] Wang SQ, Mayer JW. J Appl Phys 1990;67:2933.
- [6] Pretorius R, Harris JM, Nicolet M-A. Solid-State Electron 1978;21:667.
- [7] Ndwandwe OM, Hlatshwayo QY, Pretorius R. Mater Chem Phys 2005;92:487.
- [8] Hunter D, Osborn W, Wang K, Kazantseva N, Hattrick-Simpers J, Suchoski R, et al. Nat Commun 2011;2:518.
- [9] Williams DB, Carter CB. Transmission electron microscopy: a textbook for materials science. New York: Plenum; 2009.
- [10] Egerton RF. Electron energy-loss spectroscopy in the electron microscope. 3rd ed. New York: Plenum; 2011.
- [11] Bragg WL, Brown GB. Z Kristallogr 1926;63:538.
- [12] Ohnuma S, Kobayashi N, Fujimori H, Masumoto T, Xiong XY, Hono K. Scr Mater 2003;48:903.
- [13] Raghavan V. Ind Inst Metal 1989;5:82.
- [14] Selleby M. Metal Mater Trans B 1997;28B:563.
- [15] Raynor GV, Rivlin VG. Inst Metal Lond 1988;4:256.
- [16] Ustinovshikov Y, Pushkarev B. J Alloys Compd 2006;424:145.
- [17] Lumpkin GR, Ribbe PH. Am Mineral 1983;68:164.
- [18] Nomura S, Santoro R, Fang J, Newnham R. J Phys Chem Solids 1964;25:901.
- [19] Lottermoser W, Fuess H. Phys Status Solidi (a) 1988;109:589.
- [20] Kattner UR, Campbell CE. Mater Sci Technol 2009;25:443.
- [21] Tanaka T, Hara S. Z Metallkd 2001;92:1236.
- [22] Burlakov VM, Briggs GAD, Sutton AP, Bongiorno A, Pasquarello A. Phys Rev Lett 2004;93:135501.
- [23] Kumar H, Ghosh S, Srivastava P, Kabiraj D, Avasthi DK, Olivi L, et al. Adv Mater Lett 2012. doi: <http://dx.doi.org/10.5185/amlett.2012.ib.101>.
- [24] Andersson J-O, Helander T, Höglund L, Shi P, Sundman B. CALPHAD 2002;26:273.
- [25] Jung I-H, Deckerov SA, Pelton AD. Int J Mater Res 2007;98:816.
- [26] SGTE, Landolt-Börnstein, Group IV. Thermodynamic properties of inorganic materials compiled by SGTE, Subvol. A Pure Substances, vol. 19. Berlin: Springer Verlag; 1999.
- [27] SGTE, Landolt-Börnstein, Group IV. Thermodynamic properties of inorganic materials compiled by SGTE, Subvol. B Binary Systems, vol. 19. Berlin: Springer Verlag; 2002.
- [28] Gurvich LV, Veyts IV, Alcock CB. Thermodynamic properties of individual substances. 4th ed. New York: Hemisphere; 1990.
- [29] Raghavan V. The Co-Fe-O (Cobalt-Iron-Oxygen) system, phase diagrams ternary iron alloys. Indian Inst Met 1989;5:82–8.

- [30] Villars P, Price A, Okamoto H, editors. Handbook of ternary alloys phase diagram. Materials Park (OH): ASM International; 1995.
- [31] Raghavan V. The Fe-O-Si (Iron-Oxygen-Silicon) system, phase diagrams ternary iron alloys. Indian Inst Met., Vol.(5), 1989;5:260–77.
- [32] Sundman B. J Phase Equilib 1991;12:127.
- [33] Chen M, Hallstedt B, Gaukler LJ. J Phase Equilib 2003;24:212.
- [34] Thermo-Calc Database Guide. Stockholm (Sweden): Thermo-Calc Software AB; 2006.